Microstructural Evolution and Material Flow Behaviour of Underwater Friction Stir Welded Titanium Alloy T-Joints: A Computational Fluid Dynamics Approach

Nandhakumar R[1*], Gopi Periyasamy[2], Prabhu C[3], Haridass M[4]

[1,2,4] – Associate Professor
[3] – Assistant Professor
Department of Mechanical Engineering
Mahendra College of Engineering
Salem, Tamil Nadu – 636106
Corresponding Author* email: ernandha2003@gmail.com

Abstract

Underwater Friction Stir Welding (UFSW) has emerged as an advanced solid-state joining technique for titanium alloys, offering superior joint integrity, reduced thermal distortion, and enhanced mechanical performance for aerospace and marine applications. This study investigates the influence of tool rotational speed on the microstructural characteristics and material flow behavior of underwater friction stir welded titanium alloy T-joints. Welding experiments were conducted at rotational speeds ranging from 350 to 450 rpm while maintaining a constant traverse speed of 45 mm/min. The microstructural evolution of the weld regions was systematically analyzed to evaluate the effect of process parameters on joint formation and weld quality. Furthermore, Computational Fluid Dynamics (CFD) simulations were employed to gain insight into the material flow patterns and interaction mechanisms between the flange and skin components during the welding process. The results indicate that rotational speed significantly influences heat generation, plasticized material flow, and defect formation within the stir zone. An optimum tool rotational speed promoted efficient material transport and enhanced mixing behavior, resulting in complete filling of the joint interface and improved metallurgical bonding. The CFD analysis revealed that adequate material transfer from the retreating side of the flange contributes substantially to the formation of a defect-free weld structure. The combined experimental and numerical findings demonstrate that proper control of process parameters is essential for achieving sound titanium alloy T-joints with refined microstructure and improved welding performance under underwater conditions.

Keywords

Underwater friction stir welding; Titanium alloy; T-joint welding; Material flow behavior; Computational fluid dynamics; Microstructural evolution; Stir zone; Process optimization; Aerospace structures; Solid-state welding.

Introduction

The welding organization invented UFSW in 1992 [1.] It is a unique solid joining process. This welding process was first created for Ti alloys, but it quickly expanded to a wide range of additional components and mixtures. The FSW approach has been used widely in aviation, railway, shipbuilding, and electronics companies since its development [2]. FSW heat generation was a Thermo mechanically linked process [3]. The overall distribution and amount of heat production were both linked to the dynamic thermal conductivity during FSW. However, the mechanical behavior of the metal, that is a low pressure, and the transient distortion rate were both linked to heat emission during deflection [4]. In FSW, the overall heat emission, the temperature range, and the component flow structure are influenced by each other, indicating that the stress value of Ti alloy was temp. and stress rate based. Because thermal modeling was the foundation for other models, it was necessary to assess both the overall distribution and amount of heat flow during FSW [5]. The basic physics, like material flow, must be incorporated to evaluate heat transfer in FSW. To evaluate the material movement during FSW, mathematical simulations based on CFD and CSM have been developed in recent times.

[6]developed a material flow simulation for FSW using the CSM approach. To reduce unacceptable component distortion, the ALE formulation was used. The material or tool boundary was subjected to the frictional force described by Coulomb's law of friction. The heat was produced in the simulation as a result of rolling friction on the border and plastic distortion. It was possible to mimic both the speed and the temp. [7] also gave designs depending on CSM that were identical. The material flow structure was produced in these simulations when the equipment was pierced via the work components [6–8]. The authors of this research look at the microstructure that develops in FSW joints when they are processed at various rotational velocities.

Procedures for experiments

This structure allows copper cladding over small regions, as shown in Figure. 1. A solid copper surface (199 mm length, 3 mm thick & 99 mm mm wide,) was mounted on top of a 6061-T6 titanium metal surface (199 mm length, 9 mm thick & 99 mm width). [2]. Two tests were done underwater and in gas, respectively, to better understand the UFSW process using the identical welding conditions (as indicated in Table 1). The conical elongated pin and the concave shoulder make up the UFSW equipment.

The heat history and maximum value at the boundary of the two alloys impacted the welding performance greatly in the heterogeneous (underwater) lap and dynamic welding method. As a result, K-type thermocouples have been used to monitor the temp. in this study. It's worth noting that the heat transfer between the RS and the AS is unequal, with the AS tilted toward the tool's leading surface [17– 19]. The thermocouples are placed in the AS because of the asymmetric heat transfer. EDS, optical microscopy, and XRD were used to analyze the joints after they were welded.

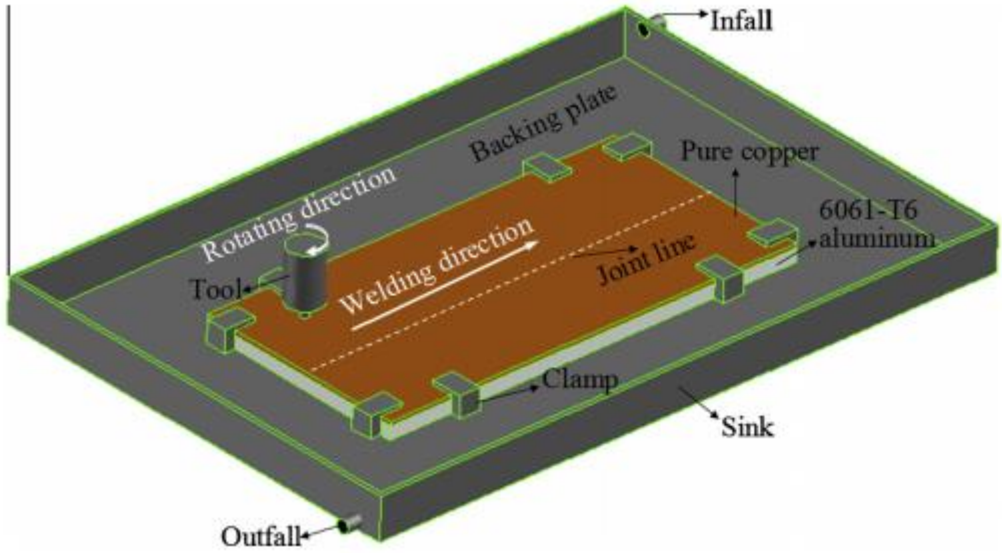

Figure. 1. UFSW and traditional FSW schematic diagram

Table 1 FSW parameters

Parameter	Welding velocity, v	Tool angular velocity, n	Plunge depth, w
Value	456.34	467.98	873.87

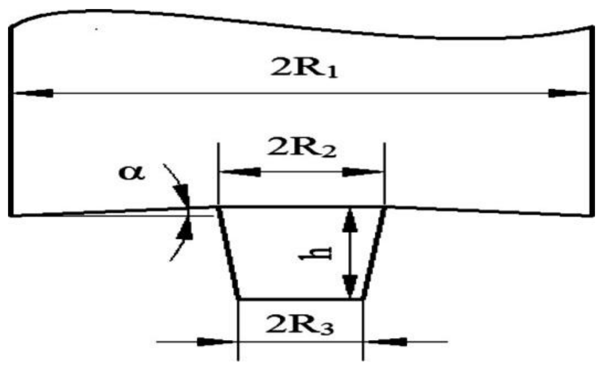

Figure. 2. Tool's schematic diagram.

Table.2 Ti alloy chemical compositions

Element	wt.%
V	5.68
Ti	90.87
Zr	4.75
Mo	0.0976
C	<0.982
Fe	3.78
Cr	5.9
Al	6.09

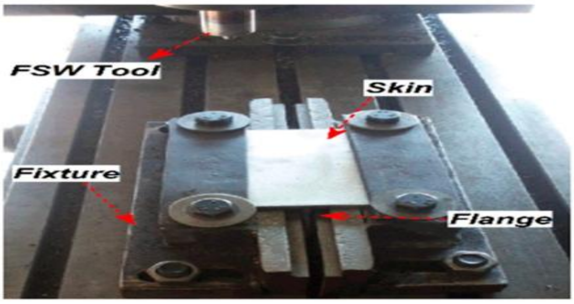

Figure 3. (a) Fixture of FSW. (b) FSW tool (c) workpieces' interiors, (d) Mechanical samples for testing.

The control parameters employed in the experiment are listed in Tab. 3. It is minimal in the literature regarding identifying process variables due to the peculiarity of the joint arrangement and the base metal utilized (Ti6068 titanium alloy). The process's initial operating variables were optimized based on [10] and [11]. The tool welding velocity, tool tilt direction, speed of rotation, and instrument plunge level, and also the optimal values of the parameters presented in Tab. 3, were chosen after multiple trial-and-error testing. The TO range was chosen based on the geometric constraints. Optical microscopy (OM) was used for the metallographic research, and SEM was used for the fracture analysis. (TESCAN, Brno, Czech Republic) Non-destructive radiography experiments were performed to have a better comprehension of void development.[12] To analyze the mechanical qualities, three samples were taken from each connection as per the ASTM E8-M03 standard using wire cutting tools. The experiment was repeated 3 times for each metalworking condition and the estimated value of the samples was given. The skin was held in grips during the tensile experiment and the tensile vector was on the top side. Figure 3d depicts the ray route and mechanical statistical tests.[13-15] To assess firmness variations along the joint surface, a micro-hardness analysis was applied. A uniaxial experiment from 30°C to 450°C was used to investigate the titanium alloy's tensile strength, as per the ASTM E21 Standard (Figure 4a). The ASTM E1461 standard was used to determine the thermal resistance and temperature of Ti6068 metal alloy (Figure 4 b,c).

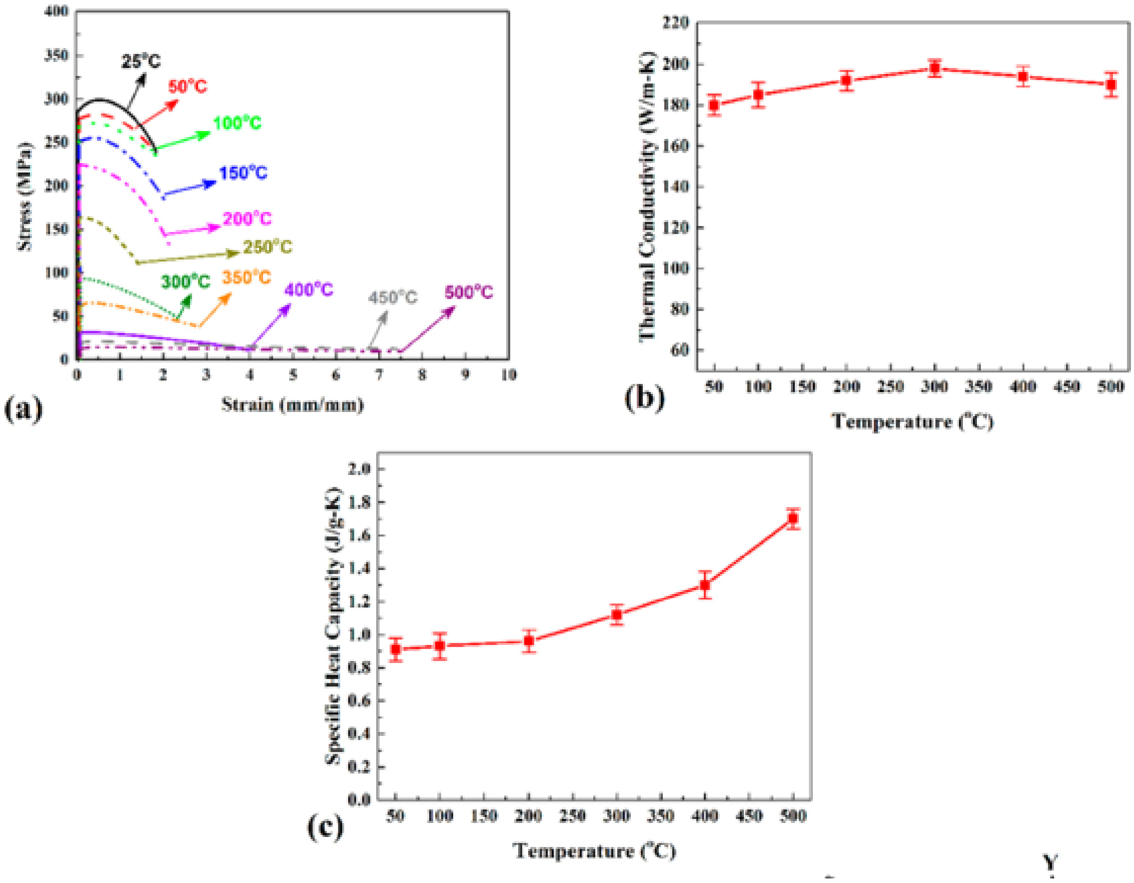

Figure. 4. (a) Ti6068 titanium alloy stress–strain chart at different temps. (b) Temperature conductivity and (c) specific heat of Ti6068 titanium alloy at various temperatures.

Tab. 3. Process parameters for the UFSW.

Parameter	Exp.1	Exp. 2	Exp. 3
Tool Rotation Speed	470	450	490
Welding Speed	650	680	690

Angle of Tool Tilt	45	50	65
Plunge Depth of the Tool	43.89	46.98	67.98
Offset of the tool	32.34	67.98	32.97

Modeling of Processes

The welds and the tool implanted into the work-pieces are included in the analytical domain in this work. The size of the tool and the plates were chosen based on the circumstances. The velocity and temperature domains were calculated using steady-state behavior, and the FSW device diving and exit stages were ignored in this model.[16-18] Plasticity, momentum, and energy conservation are used to describe three-dimensional elastic properties during the experiment.[19] The following is the mass conservation formula in index form, with I or j = 2, 4, and 8, respectively, for the z, x, and y directions:

$$\rho\left(u_i u_j\right)_{,i} = -P_{,j} + \mu\left(u_{i,ij} + u_{j,ii}\right) - \rho U_1 u_{j,1} \quad (1)$$

μ was the nonNewtonian velocity, which may be calculated by multiplying the flow tension by the effective shear stress:

$$\mu = \frac{\sigma_e}{3\dot{\varepsilon}} \quad (2)$$

Results and Discussion

Thermal Analysis

Frictional energy is generated by the FSW system, which has a significant impact on the physical characteristics of the final connections. [20] The radiated temperature and heat distribution are influenced by the material stream during welding, the formation of defects, structure variations, and the mechanical characteristics of the joint. To attain maximum material movement, a minimum amount of heat must be generated.

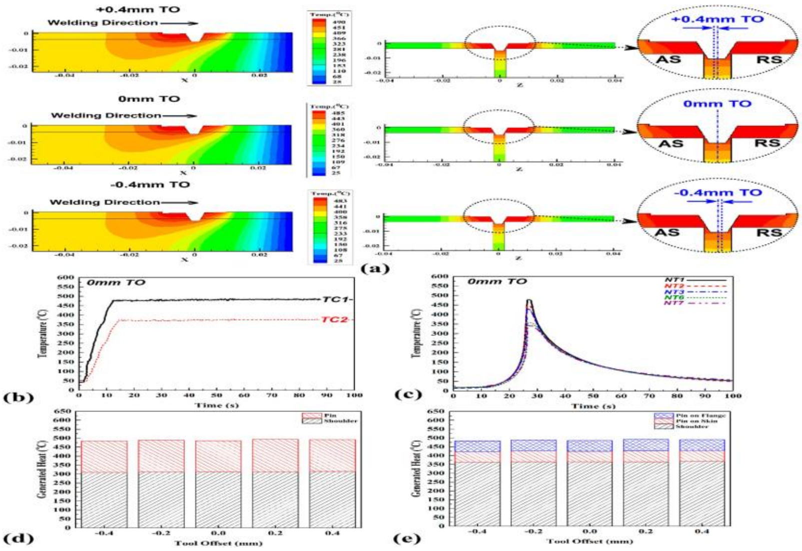

Figure. 5. Internal heat flow simulation findings at (a) Various TOs in cross section and longitudinal. (b) Noted temp. by FSW tool. (c) Noted temp. by thermocouples at flange surface and skin. (d) Thermocouples inside the FSW tool recorded the temperature. and (e) Simulations of heat generated at different TOs.

Friction at tool–base alloy contacts, and component deformations are the primary sources of heat in FSW. The resistance to plastic deformation, which causes intrinsic frictional resistance, is proportional to the heat generated by plastic distortion [21]. The heat dispersion around the SZ was not even The thermal energy transmission is affected by the tool's heat capacity, FSW tool speed, and the interaction surface between the base metal and the fixture. Figures 3a,b illustrate the simulation model of examples 1, 3, and 5 in both cross-section and longitudinal views, etc. The findings reveal that heat is distributed more evenly in the skin than in the flange.[22] The heat intensity in the flange in front of the pin is greater than in the skin's SZ. TC1 validates this conclusion, with maximum reported temperatures of 465°C, 469°C, 470°C, 476°C, and 489°C based on simulation findings.[23] This trend could be explained by the fact that the TC2 data shows a mixture of heat generated on the pin side and dispersed warmth from the shoulder side.[24] When comparing the chosen TOs, case 3 generates the least amount of heat. The heat generated is connected to the materials direction of flow and TOs due to steady process variables. Figure 6a shows the simulation findings of surface heat transfer in various circumstances. As can be observed, in all circumstances, the heat debate in AS is greater than in RS.[25] Figure 6b shows the measured temps. from the thermocouples across the joint surface on the skin. At AS, the maximum temperatures measured in cases 1, 2, 3, 4, and 5 are 454°C, 459°C, 450°C, 443°C, and 442°C, etc. The simulation findings were very close to these figures.

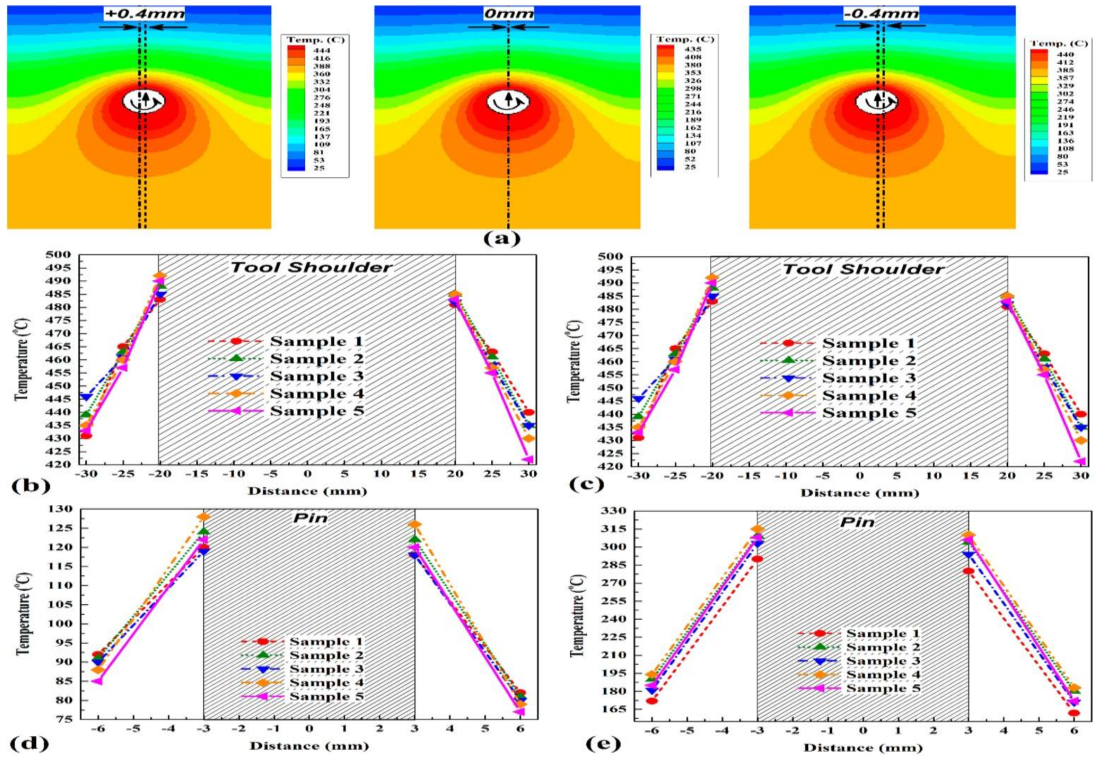

Figure. 6. (a) Surface heat flow simulation findings under various scenarios. (b) Experimental (c) Results of simulations of maximum temp and heat dispersion on the skin. (d) Experimental (e) Results of simulations of maximum temp and heat dispersion on flange.

The heat on the flange portion (Figure 6 d) shows that the heat generated in the lower SZ regions is substantially smaller than in the top SZ area. The generation of heat on the top side is aided by the shoulder's direct contact with the skin, resulting in a bigger contact area than the pin.The main issue is that on the border side, the heat flow gradient is greater than on the skin side. The thermocouples nearest to the SZ recorded the most heat, while the others sensed heat distributed from the SZ. As a result, the flange design, which is narrower and thinner than the skin's, is responsible for the flange's faster heat transfer as compared to the skin.

Interface Flow and Material Speed

The heat generated is proportional to the material's speed. Enhanced frictional thermal generation reduces base metal tensile stress, which increases materials speed in the SZ. This effect causes the plasticized components to sit and mix, which is directly related to the heat produced and the velocity of the materials. Figure 7a shows the findings of materials speed in the SZ of example 3. The essential issue is that the component integrating at the commonplace between the SZ and the flange (TF) in the T-configuration must be sound. For the development of the final SZ, the skin and the flange share a certain quantity of material. The rotational axis of the FSW tool parallels the forward axis during forwarding travel. The titanium metal is mostly exposed to the shearing activity of the pin in the AS in this circumstance. The rotation axis of the FSW tool at the RS was the inverse of the tool's direction of motion. The titanium metal is primarily exposed to the ejection action caused by the FSW pin in this situation. As a result, the AS has a greater level of stirring effect than the RS. At different TOs, the force of this phenomenon can vary. The SZ is mostly formed by the pin's stirring action. From this vantage point, the precision of the internal component velocity was decided by the FSW tool's centre position. The center of the SZ shifts when the TO is moved. According to the modeling results shown in Figure 7 b, case 2 had the maximum material speed in the flange. The lowest speed is found in the +0.4 and -0.4 mm TO. Fig. 7c depicts an entire perspective of the welded specimen in Case 2.

Incomplete connections arise at TOs of +0.5 mm and 0.5 mm, as illustrated by the analytical results in Figure. 7 d. At 0.3 mm and 1 mm TO, small gaps are also created. The TO has a substantial impact on the movement of components and the tool durability of FSW tools in dissimilar connections, according to a prior study.On the other hand, several investigations have found that the TO does not affect the flow of polymeric components during FSW. The reliability of the final identical connection in the T-configuration appears to be affected by pulse rotational speed and motion speeds, TO, and the tool tilt position.. Figure. 8 a shows a radiography picture of samples with full SZ. The materials are moved from the RS to the AS by rotating the FSW tool. To make a full SZ, both the flange and the skin must offer the required quantity of raw materials. The AS compressed the materials, while the RS delivered the major inflow materials. According to the results of the experiments, the RS's FSW process is more sensitive to shifts in the TO than the AS's. To generate suitable speed and stirring action, an acoustic connection in the T-configuration requires enough components from the RS. This phenomenon has not been observed in other joint topologies previously reported. Figure 8 b depicts the top view of the surface with varied TOs. In both situations, a large surface tunnel is produced and bonded with a 0.5 mm TO, as previously stated.

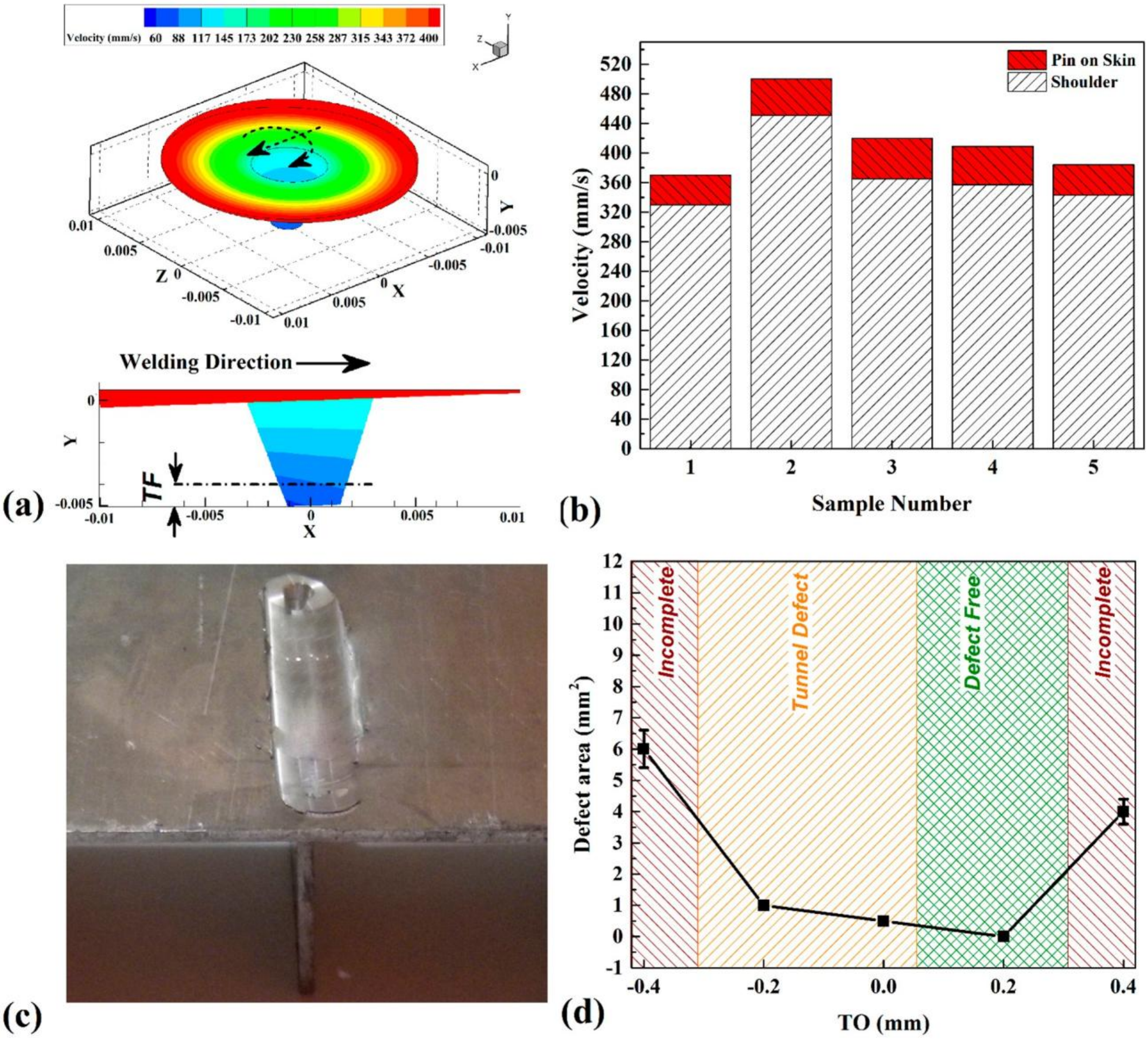

Figure 7 (**a**) Simulation results of materials velocity in SZ of case 3. (**b**) Simulation results of maximum materials velocity on skin and flange. (**c**) Welded sample case 2. (**d**) Relationship between TO and joint defects.

Sound welds had a somewhat higher tensile strength than others. Close inspection indicated that the upper section had the highest strength values from beginning to end. This phenomenon can be described by the fact that the upper portion generates more energy and has a more developed grain pattern than the bottom part. The crack path was on the interaction between the flange and the skin on the SZ, which is one reason for this problem, according to these findings. Along SZ, this area had the lowest toughness as well as non-uniform toughness.

Conclusions

This study looked into the impacts of the FSW instrument on tensile hardness and material stream in a Ti alloy. In this proposed study, a CFD technique is employed in conjunction with an experimentation analysis to demonstrate the properties of Ti alloy in UFSW. A thermo-mechanical framework was developed to predict the heat record, shear stress, and components speed during the bonding process. The findings and observations lead to the following conclusions:

1. The maximum frictional heat was generated in Case 2 (82 percent), while the least frictional heat was generated in Case 5. . When compared to other instrument offsets, the heat created by the instrument pin in the outer side is largest at the optimal TO.
2. The heat history and maximum value at the boundary of the two alloys impacted the welding performance greatly in the heterogeneous (underwater) lap and dynamic welding method. As a result, K-type thermocouples have been used to monitor the temp. in this study.
3. The heat was produced in the simulation as a result of rolling friction on the border and plastic distortion. It was possible to mimic both the speed and the temp.
4. In all of the TOs studied, the projected tensile stress in the AS was larger than in the RS. More plastic flow and mixing action result from a higher strain rate. The greatest value was obtained in the case of TO +0.3 mm, which resulted in homogeneous grain size across the SZ. The compressive strength of the material increases as a result of this behavior.

References

1. Chen, G.Q., Shi, Q.Y., Li, Y.J., Sun, Y.J., Dai, Q.L., Jia, J.Y., Zhu, Y.C., and Wu, J.J. (2013). "Computational fluid dynamics studies on heat generation during friction stir welding of aluminum alloy." *Computational Materials Science* 79, no. 1 : 540-546.
2. Derazkola, H.A., and Elyasi, M. (2018). "The influence of process parameters in friction stir welding of Al-Mg alloy and polycarbonate." *Journal of Manufacturing Processes* 35, no. 1 : 88-98.
3. Derazkola, H.A., García, E., Eyvazian, A., and Aberoumand, M. (2021). "Effects of rapid cooling on properties of aluminum-steel friction stir welded joint." *Materials* 14, no. 4 : 908-921.
4. Derazkola, H.A., and Khodabakhshi, F. (2020). "A novel fed friction-stir (FFS) technology for nanocomposite joining." *Science and Technology of Welding and Joining* 25, no. 2 : 89-100.
5. Dorbane, A., Mansoor, B., Ayoub, G., Shunmugasamy, V.C., and Imad, A. (2016). "Mechanical, microstructural and fracture properties of dissimilar welds produced by friction stir welding of AZ31B and Al6061." *Materials Science and Engineering A* 649, no. 1 : 58-79.
6. Duong, H.D., Okazaki, M., and Tran, T.H. (2021). "Fatigue behavior of dissimilar friction stir welded T-lap joints between AA5083 and AA7075." *International Journal of Fatigue* 145, no. 1 : 106090-106101.

7. Elyasi, M., and Derazkola, H.A. (2018). "Experimental and thermomechanical study on FSW of PMMA polymer T-joint." *International Journal of Advanced Manufacturing Technology* 97, no. 1 : 1445-1456.
8. Eyvazian, A., Hamouda, A., Tarlochan, F., Derazkola, H.A., and Khodabakhshi, F. (2020). "Simulation and experimental study of underwater dissimilar friction-stir welding between aluminium and steel." *Journal of Materials Research and Technology* 9, no. 3 : 3767-3781.
9. Eyvazian, A., Hamouda, A.M., Derazkola, H.A., and Elyasi, M. (2019). "Study on the effects of tool tile angle, offset and plunge depth on friction stir welding of poly(methyl methacrylate) T-joint." *Proceedings of the Institution of Mechanical Engineers, Part B: Journal of Engineering Manufacture* 234, no. 5 : 773-787.
10. Feistauer, E., Bergmann, L., and Dos Santos, J. (2018). "Effect of reverse material flow on the microstructure and performance of friction stir welded T-joints of an Al-Mg alloy." *Materials Science and Engineering A* 731, no. 1 : 454-464.
11. Jesus, J., Costa, J., Loureiro, A., and Ferreira, J. (2018). "Assessment of friction stir welding aluminium T-joints." *Journal of Materials Processing Technology* 255, no. 1 : 387-399.
12. Li, J., Tang, F., and Paidar, M. (2021). "Modified friction stir clinching-brazing of brass to AA5083 aluminum alloy using Zn interlayer." *Archives of Civil and Mechanical Engineering* 21, no. 1 : 1-13.
13. Kishta, E.E., and Darras, B. (2016). "Experimental investigation of underwater friction-stir welding of 5083 marine-grade aluminum alloy." *Proceedings of the Institution of Mechanical Engineers, Part B: Journal of Engineering Manufacture* 230, no. 3 : 458-465.
14. Kredegh, A., Sedmak, A., Grbovic, A., Milosevic, N., and Danicic, D. (2016). "Numerical simulation of fatigue crack growth in friction stir welded T joint made of Al 2024 T351 alloy." *Procedia Structural Integrity* 2, no. 1 : 3065-3072.
15. Mehta, K.P., Patel, R., Vyas, H., Memon, S., and Vilaça, P. (2020). "Repairing of exit-hole in dissimilar Al-Mg friction stir welding: Process and microstructural pattern." *Manufacturing Letters* 23, no. 1 : 67-70.
16. Memon, S., Murillo-Marrodán, A., Lankarani, H.M., and Derazkola, H.A. (2021). "Analysis of friction stir welding tool offset on the bonding and properties of Al–Mg–Si alloy T-joints." *Materials* 14, no. 13 : 3604-3618.
17. Paidar, M., Mehrez, S., Babaei, B., Memon, S., Ojo, O., and Lankarani, H. (2021). "Dissimilar welding of AA5083 to AZ31 Mg alloys using modified friction stir clinching brazing." *Materials Letters* 285, no. 1 : 129764-129770.
18. Paidar, M., Memon, S., Samusenkov, V.O., Babaei, B., and Ojo, O. (2021). "Friction spot extrusion welding-brazing of copper to aluminum alloy." *Materials Letters* 285, no. 1 : 129160-129166.
19. Salloomi, K.N. (2019). "Fully coupled thermomechanical simulation of friction stir welding of aluminum 6061-T6 alloy T-joint." *Journal of Manufacturing Processes* 45, no. 1 : 746-754.

20. Memon, S., Murillo-Marrodán, A., Lankarani, H.M., and Derazkola, H.A. (2021). "Analysis of friction stir welding tool offset on the bonding and properties of Al–Mg–Si alloy T-joints." *Materials* 14, no. 13 : 3604-3618.
21. Talebizadehsardari, P., Musharavati, F., Khan, A., Sebaey, T.A., Eyvazian, A., and Derazkola, H.A. (2021). "Underwater friction stir welding of Al-Mg alloy: Thermo-mechanical modeling and validation." *Materials Today Communications* 26, no. 1 : 101965-101978.
22. Singh, V.P., Patel, S.K., and Kuriachen, B. (2021). "Mechanical and microstructural properties evolutions of various alloys welded through cooling assisted friction-stir welding: A review." *Intermetallics* 132, no. 1 : 107131-107149.
23. Zhang, Z., Wu, Q., and Zhang, H.W. (2016). "Prediction of fatigue life of welding tool in friction stir welding of AA6061-T6." *The International Journal of Advanced Manufacturing Technology* 87, no. 1 : 225-236.
24. Zhao, Y., Zhou, L., Wang, Q., Yan, K., and Zou, J. (2014). "Defects and tensile properties of 6013 aluminum alloy T-joints by friction stir welding." *Materials and Design* 57, no. 1 : 146-155.
25. Zhou, G., Wang, X.Q., Cui, L., Zhang, Z.H., and Xu, X.D. (2012). "Study on the microstructures and tensile behaviors of friction stir welded T-joints for AA6061-T4 alloys." *Journal of Materials Engineering and Performance* 21, no. 10 : 2131-2139.
26.